Journal of Colloid and Interface Science 502 (2017) 201–209

Contents lists available at ScienceDirect

Journal of Colloid and Interface Science

journal homepage: www.elsevier.com/locate/jcis

Regular Article

Plasmonic/magnetic nanocomposites: Gold nanorods-functionalized silica coated magnetic nanoparticles

Eugenio Redolfi Riva [a,*], Isabel Pastoriza-Santos [b], Aidin Lak [c], Teresa Pellegrino [c], Jorge Pérez-Juste [b], Virgilio Mattoli [a,*]

[a] Center for Micro-BioRobotics, Istituto Italiano di Tecnologia, 56025 Pontedera, Italy
[b] Departamento de Química Física-CINBIO, Universidade de Vigo, Vigo 36310, Spain
[c] Istituto Italiano di Tecnologia, Via Morego 30, Genova, Italy

GRAPHICAL ABSTRACT

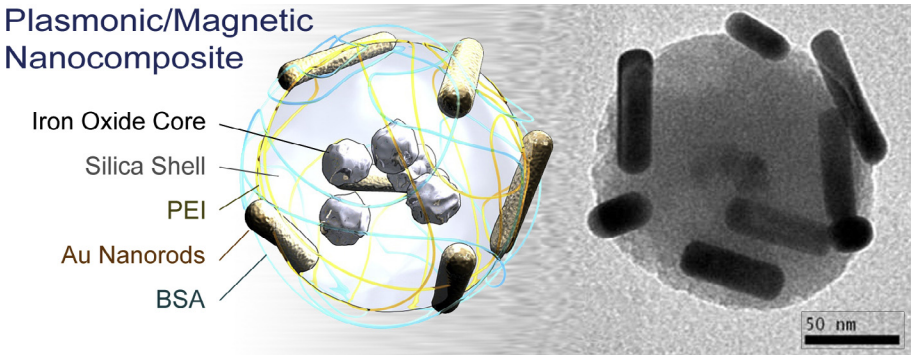

ARTICLE INFO

Article history:
Received 10 March 2017
Accepted 27 April 2017
Available online 28 April 2017

Keywords:
Gold nanorods
Magnetic nanoparticles
Plasmonic nanoparticles
Photothermal therapy

ABSTRACT

We report here on the fabrication of a new example of nano-object that combines magnetic and plasmonic properties. The strategy is based on the electrostatic assembly of negatively charged gold nanorods (NIR-resonant) on positively charged silica-coated iron oxide nanoparticles. Silica coating of magnetic nanoparticles prevented iron oxide nanoparticles irreversible aggregation in water environment. Finally the stability of the nanocomposite in biological medium has been improved through a protein coating (BSA, bovine serum albumin). Morphological, optical and magnetic properties of the hybrid nanomaterials have been evaluated as well as its ability to be manipulated by an external magnetic field. Furthermore, temperature characterization upon NIR laser excitation has been performed in order to assess nanocomposite capability of increasing local environmental temperature. This nanomaterial could be used as a smart tool for photothermal treatment of cancerous lesions in order to maximize precision and efficacy of tissue heating upon laser stimulation by magnetically accumulating nanoparticles nearby the cancerous lesion, avoiding dispersion of the nanomaterial.

1. Introduction

Surface Plasmons (SPs) are collective oscillations of surface electrons of a metal that possess an energy, a momentum and a propagation direction. Light can interact with SPs and being either

* Corresponding authors.
E-mail addresses: eu.redriva@gmail.com (E. Redolfi Riva), virgilio.mattoli@iit.it (V. Mattoli).

http://dx.doi.org/10.1016/j.jcis.2017.04.089
0021-9797/

reflected or absorbed by the material if its frequency is below or above the plasma oscillation frequency, respectively. For materials such as gold and silver, when the wavelength of the incident radiation is higher than their dimensions, light interaction with SPs produces a resonance condition characterized by intense light scattering, appearance of surface plasmon absorption bands and enhancement of the local electric fields [1]. In the case of a material with a planar surface this phenomenon is called Surface Plasmon Resonance (SPR), whereas for nanostructured materials, such as a nanoparticle, this occurrence is named Localized Surface Plasmon Resonance (LSPR). SPs are strongly influenced by either the nature or the geometry and size of the material. Therefore by tailoring the shape and dimension of the nanoparticles one can finely tune their optical properties, such as plasmon resonance frequency and absorption efficiency [2].

In the last decades nanoplasmonics has paved the way to the possibility to fabricate metallic nanoparticles with finely tunable optical properties. Several examples of different shape nanomaterials such as gold nanospheres, nanocubes, nanostars, nanorods and nanowires have been presented [3–8] and their plasmonic properties have been exploited for various biomedical applications, such as diagnosis, detection and cancer photothermal therapy [9,10]. As an example, detection of biomolecules can be carried out by Surface Enhanced Raman Scattering (SERS) spectroscopy using gold or silver colloids as plasmonic platforms that directly bind the target analyte. Plasmonic platforms generates a huge near electric field which produces a strong enhancement (up to 10^{14} factor) of the biomolecule Raman signal allowing its detection even at relative low concentrations [11,12]. Gold nanostars have demonstrated to be particularly efficient for SERS-based detection because of the confinement of the electric field at the nanoparticles tips which greatly increases the sensibility for analyte detection via SERS [13].

LSPRs centered in the Near Infrared (NIR) region is a very promising tool for biomedical application, such as molecule detection and for photothermal therapy, thanks to high tissue penetration and low absorption coefficient of NIR photons. Regarding photothermal therapy, high absorption cross section of NIR photons by gold nanoshells allows energy conversion into heat upon laser irradiation of the tissue portion where particles are located [14–20]. This technique ensures complete cancer cell destruction by irreversible membrane stress of even deeply located lesions, since low NIR absorption by biological tissue that allows larger light penetration. However, difficulties of particles localization in the desired area and lack of efficient cancer cell targeting limit the clinical use of photothermal therapy for cancer ablation, since either unpredictable and inefficient heat transfer occurs in correspondence of the region of particles localization [21,22].

A possible solution to this issue could be adding magnetic properties to plasmonic nanoparticles in order to be able to control their accumulation in a desired area of the body through an external static magnetic field gradient upon intravenous injection. In this scenario, a plasmonic/magnetic PlasMag nanocomposite combining plasmonic and magnetic nanoparticles could be a promising solution to the issue of inefficient tissue heating, since it could enhance particles accumulation nearby the tumor region. In literature, examples of the possibility to coupling magnetic and plasmonic properties have been reported. For instance Heyon et al. in 2006 reported the fabrication of magnetic gold nanoshells by functionalizing silica nanoparticles with iron oxide nanoparticles and then growing a gold shell onto this assembly [23]. Superparamagnetic behavior and NIR-resonant optical properties have been demonstrated, as well as, the possibility to kill cancer cell in vitro by NIR laser stimulation. A similar approach was adopted by Haam et al., where iron oxide nanoclusters were first silica-coated and then a gold shell was further growth [24]. However, Mie-based calculations performed for various gold nanoparticles reported by M. El-Sayed showed higher NIR absorption coefficient for gold nanorods (AuNRs) with respect to gold nanoshells at various dimensions, concluding that gold nanorods seems more efficient particles for photothermal application [25]. Therefore, in our work we present a new concept of PlasMag made by silica-coated iron oxide nanoparticles assembled with NIR-resonant gold nanorods. AuNRs have been selected because of their small dimensions and higher absorbance efficiency with respect to nanoshells. It allows the fabrication of small nanocomposites combining magnetic drivability and good optical properties. Electrostatic attraction between negatively charged gold nanorods and positively charged silica-coated nanoparticles has been used as driving force for nanoparticles assembly. Apart from its fabrication and its optical and magnetic properties we have also investigated the ability to increase local temperature upon NIR laser stimulation. This material could be used as promising tool for photothermal ablation of deeply located tumor masses upon magnetic accumulation nearby the targeted area.

2. Materials and methods

2.1. Materials

Tetrachloroauric acid ($HAuCl_4 \times 3H_2O$), tetraethylorthosilicate (TEOS), ammonium hydroxide (NH_4OH, 28%) were purchased from Aldrich. Ascorbic acid, silver nitrate ($AgNO_3$), sodium borohydride ($NaBH_4$) and poly(styrenesulfonate) (PSS, M_W 70,000) polyethylenimine (PEI, Fluka, 50% (w/v)) were supplied by Sigma. Cetyltrimethylammonium bromide (CTAB) was procured from Fluka. HCl (37%) was supplied by Panreac. All chemicals were used as received. Pure grade ethanol and Milli-Q grade water were used in all preparations.

2.2. PlasMag nanocomposite fabrication

2.2.1. Gold nanorods fabrication and polyelectrolyte functionalization

Gold nanorods (AuNRs) have been produced as previously reported [26], introducing some modifications. Briefly, small gold seeds were prepared by gently mixing 250 μL of 0.01 M $HAuCl_4$ in water and 10 mL of an aqueous solution of 0.1 M CTAB. Next, 600 μL of 0.01 M $NaBH_4$ in water was quickly added at room temperature and vigorously stirred for 2 min, after which a change in the solution color from orange to gold-plated was observed. The resulting growth solution was left undisturbed at room temperature for 2 h before use it.

A growth solution was then prepared as follows: 20 mL of an aqueous 0.01 M $HAuCl_4$ solution and 4.25 mL of an aqueous 0.01 M $AgNO_3$ solution were added in 400 mL of 0.1 M CTAB in water, mixed vigorously and left undisturbed at room temperature for 15 min. After that 3.2 mL of 0.1 M ascorbic acid and 8 mL of 1 M hydrochloric acid (both in water) were added and vigorously mixed. Finally, 960 μL of seed solution were added in the so prepared growth solution, vigorously mixed and left overnight at room temperature. The obtained Au NRs were washed by centrifugation at 7000 rpm for 30 min and redispersed in an aqueous CTAB (1 mM) solution and conserved at room temperature for further use.

Surface functionalization of Au NRs with polyelectrolyte was performed using a layer by layer approach based on electrostatic interactions [27]. Briefly, a PSS (2 mg/mL, 6 mM NaCl) aqueous solution was prepared and sonicated for at least 15 min to allow polymer chains complete distension. Then 25 mL of Au NRs solution was washed by centrifugation at 4500 rpm for 45 min, redispersed in 25 mL water and finally added dropwise to 25 mL of PSS solution under stirring. After 3 h under stirring PSS-coated Au NRs were washed twice by centrifugation (first cycle:

3500 rpm for 45 min; second cycle: 2800 rpm for 45 min) and redispersed in water. Supernatant was recollected and subsequently centrifuged at 4000 rpm for 15 min to recover the remaining gold nanoparticles.

2.2.2. Silica coating and polyelectrolyte functionalization of magnetic nanoparticles

(3-Aminopropyl)triethoxysilane (APTES)-coated iron oxide nanoparticles (MagNPs) were purchased from Chemicell at the concentration of 25 mg/mL. Silica coating of MagNPs was performed following the Stöber method [28] with some modifications. Briefly 680 μL of MagNPs were sonicated for 10 min and then mixed with 2.75 mL of EtOH and 485 μL of NH_4OH (28%). Under sonication 3 mL of ethanol containing 50 μL of TEOS was added dropwise to the mixture. It was allowed to react for 90 min under sonication. Then silica-coated MagNPs, Mag@SiO_2 NPs, were washed three times (three cycles of centrifugation at 3500 rpm for 30 min and redispersed in the same volume of water).

In a next step, Mag@SiO_2 NPs were functionalized with polyethylenimine (PEI) to provide a positive charge to the nanoparticles surface. Briefly, 1 mL of Mag@SiO_2 NPs were added dropwise at the same volume of a PEI (2 mg/mL, 1 M NaCl) aqueous solution and left overnight under stirring. After that NPs were centrifuged three times at 3500 rpm for 30 min and finally redispersed in water to obtain MagNPs@SiO_2@PEI NPs. Finally a standard curve was made to calculate particle concentration by checking absorbance at 375 nm. Particle concentration has been reported as mg/mL or as number particles per mL of medium (part/mL).

2.2.3. Electrostatic assembly of gold nanorods on silica-coated magnetic nanoparticles

Electrostatic deposition of negatively charged AuNRs@PSS on positively charged Mag@SiO_2@PEI NPs was performed by mixing this two type of particles in water under sonication. Briefly, 1 mL of 1 mM AuNRs@PSS was added dropwise under sonication to a 0.9 mg/mL Mag@SiO_2@PEI colloids in water to obtain the desired complexation between AuNRs and silica-coated MagNPs. The mixture was left first under sonication for 15 min and then under mechanic agitation for other 15 min, in order to allow electrostatic assembly between nanoparticles. After this, protein coating of the material was performed using bovine serum albumin (BSA). Thus, 2 mL of the nanocomposite solution were added under sonication to 2 mL of a phosphate buffered saline (PBS) solution containing 4 mg of BSA. The resulting solution was left under sonication for 15 min and then under gentle mechanical agitation overnight. Finally, the **PlasMag@BSA** sample was centrifugated at 3500 rpm for 15 min and resuspended in fresh PBS in order to remove free BSA and not assembled AuNRs from the solution.

2.3. PlasMag characterization

2.3.1. Nanoparticles characterization

Optical properties of AuNRs and PlasMag nanocomposites were measured with an Agilent 8453 UV–vis spectrophotometer. Transmission electron microscopy (TEM) was carried out with a JEOL JEM 1010 transmission electron microscope operating at an acceleration voltage of 100 kV. Size (and thickness) distributions and standard deviations were determined by analyzing TEM images. Concentration of AuNRs in each batch was evaluated by checking the absorbance value of AuNRs solution, taking into account that experimentally an absorbance value of 0.12 at 400 nm corresponds to a gold concentration of 0.5 mM. Furthermore, number of particles per mL of solution was calculated using nanoparticles dimensions calculated by TEM imaging and gold concentration in 1 mL of AuNRs. Surface charge of nanoparticles was evaluated by checking Zeta-potential by Dynamic Light Scattering (Malvern Zetasizer Nano ZS).

Particles stability was always checked after each centrifugation cycle by light spectroscopy and was confirmed if no changes in the shape of particles longitudinal plasmon band was evidenced. For further experiment particles were dialyzed with using plastic tube with a porous membrane with 3500 kDa pore size (Pur-a-Lyzer Dyalisis Kit, Sigma-Aldrich) and lyophilized in order to determine the exact concentration of nanomaterial in solution. Magnetic behavior under external magnetic force of PlasMag nanocomposites has been assessed using a 6 mm diameter permanent Nd-Fe-B magnet (B_r = 1.32 T) placed on the bottom of a plastic slide with a built channel filled with 500 μL. The process of accumulation of PlasMag nanocomposites has been recorded in time lapse with a videocamera.

Moreover, magnetic properties of MagNPs, Mag@SiO_2 NPs and PlasMag nanocomposites were measured using an ever-cooled Magnetic Property Measurement System (*MPMS-XL*, Quantum Design). Magnetization versus magnetic field *M-H* hysteresis loops were recorded from −7 T to 7 T at 310 and 10 K. Zero-field-cooled (ZFC) and field-cooled (FC) magnetization curves were recorded at a cooling field of 50 Oe. Diamagnetic contributions were removed by performing the background measurement and subtraction. All magnetization data were normalized to the iron mass of nanoparticles.

2.3.2. Photothermal behavior of PlasMag@BSA nanocomposites under NIR laser stimulation

Environmental temperature rises upon laser stimulation of PlasMag@BSA nanocomposites has been assessed with the use of an IR thermocamera (A325sc, FLIR) and temperature profile has been analyzed with FLIR ResearchIR MAX Software (FLIR Systems). Temperature recording has been performed in two different configuration schematized in Supporting Information (Fig. S1) using a RLTMDL-808-500 NIR laser source (λ = 808 nm Roithner Lasertechnik, Vienna, Austra) collimated and focused with an output power of 70 mW. A three lens system (lenses from Thorlabs, Inc.) composed of an ACN254-050-B and an AC254-075-B (separated by a 28 mm air gap and forming a collimating system with an effective focal length of approximately 300 mm) and an AC254-050-B (as focusing element), was designed to focus the radiation output by the fiber into a 100 μm diameter spot on the sample. Laser power measurement and scattered/reflected power estimation were performed by means of a calibrated S121C Photodiode coupled to a PM100D power meter (Thorlabs Inc.).

In the first configuration (Fig. S1a) the collimated laser beam was focused on a 2 μL drop of PlasMag@BSA solution in PBS (2 mg/mL) deposited onto a plastic slide and temperature recording was performed in side view with respect to the drop. In the second configuration (Fig. S1b) the same NIR laser beam was focused on an area of a plastic slide where magnetically accumulated PlasMag@BSA colloids were previously deposited. NIR laser beam was shined after excess PBS removal resulted by nanocomposite magnetic accumulation on the bottom of the plastic slide. Temperature recording has been performed in top view of the area of PlasMag@BSA magnetic accumulation. Negative control experiments of temperature recording were performed in both the configuration shining NIR laser onto Mag@SiO_2 nanoparticles.

3. Results and discussions

Plasmonic/Magnetic (PlasMag) nanocomposite has been fabricated by deposition of PSS-functionalized AuNRs onto PEI-functionalized Mag@SiO_2 nanocomposites. A summary of the whole fabrication process is illustrated in Scheme 1. It involves the silica coating of MagNPs (I), PEI-functionalization of Mag@SiO_2 NPs (II), electrostatic assembly of PSS-functionalized AuNRs

(AuNRs@PSS) onto the Mag@SiO_2@PEI NPs (III) and finally the BSA coating of the resulting PlasMag nanocomposite.

In the following sections all the fabrication steps of this nanomaterial concerning nanoparticles synthesis and polyelectrolyte functionalization will be presented.

3.1. Gold nanorods synthesis and polyelectrolyte functionalization

Fig. 1 reports TEM images and corresponding UV–Vis-NIR absorption spectrum of AuNRs prepared for the study. The analysis of TEM images indicated that AuNRs presented 60.8 ± 10.3 nm in length (l) and 11.7 ± 3.2 nm in width (d) with a average aspect ratio, *l*/*d*, of about 5.2. Their optical properties show a narrow longitudinal plasmon band centered in the near infrared region (844 nm).

In order to favor the AuNRs assembly onto the magnetic nanoparticles, the plasmonic nanoparticles were functionalized with a negatively charged polyelectrolyte, PSS. It resulted in a drastic change in the AuNRs zeta potential from +41 mV to −47 mV. It is explained in terms of PSS adsorption on the positively charged CTAB-stabilized nanoparticles due to electrostatic forces. As shown in Fig. 1c, the PSS functionalization of Au NRs just produces a slight blue-shift of the longitudinal LSPR band from 844 nm to 823 nm without perturbing the stability of the nanoparticles (even after 15 days at room temperature.

3.2. Silica coating and polyelectrolyte functionalization of magnetic nanoparticles

Amino-functionalized iron oxide nanoparticles, MagNPs, with an average size of 17.7 ± 8.3 nm were selected as magnetic core, see Fig. 2a. DLS analysis revealed an average zeta potential of +46 mV due to the amino functionality. Before their combination with AuNRs, MagNPs were coated with silica via Stöber to prevent their aggregation in liquid, induced by their slight magnetization, and improve their chemical stability. TEM characterization of MagNPs after the silica coating, Mag@SiO_2 NPs, (Fig. 2b) shows the multiple encapsulation of magnetic nanoparticles inside well-defined silica shells which results in rather uniform Mag@SiO_2 NPs. Moreover after the coating the Mag@SiO_2 NPs are well separated each other which corroborates the improved stability of the magnetic nanoparticles at room temperature explained in terms of decrease of the saturation magnetization due to the silica coating [29]. As expected silica coating drastically changed average zeta potential, from +46 mV to −42.5 mV. In order to promote the deposition of the negatively charged AuNRs@PSS onto the magnetic nanoparticles, the silica surface was wrapped with a positively charged polyelectrolyte, PEI. The substantial change of the zeta potential from −42.5 mV to 40.7 mV confirmed the successful PEI coating without altering nanoparticles stability in water, since no aggregation was observed during time.

3.3. PlasMag nanocomposite fabrication and magnetic characterization

The deposition of PSS-functionalized AuNRs onto the PEI-functionalized Mag@SiO_2 NPs was done by simple mixing both types of colloids (AuNRs in excess) due to their oppositely charged surface, see Scheme 1. TEM confirmed the electrostatic assembly between AuNRs and MagNPs@SiO_2 nanoparticles. Fig. 3 shows the multiple deposition of AuNRs on Mag@SiO_2 NPs surface. Regarding the optical properties of the hybrid nanocomposties (Fig. 4) Vis-NIR spectra show a broadening of the longitudinal plasmon band and a slight red-shift respect to AuNRs. This occurrence

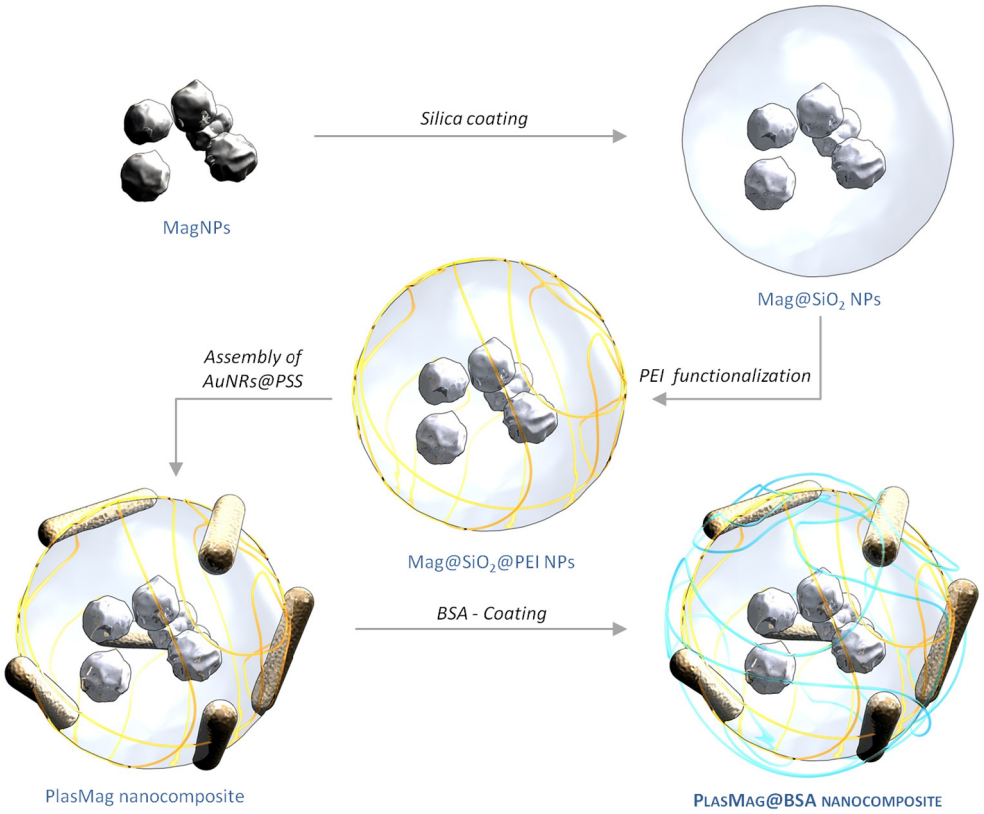

Scheme 1. Fabrication procedure of the plasmonic/magnetic nanocomposites involving the silica coating of MagNPs (I), PEI-functionalization of Mag@SiO_2 NPs (II), electrostatic assembly of PSS-functionalized AuNRs (AuNRs@PSS) onto the Mag@SiO_2@PEI NPs (III) and finally the BSA coating of the resulting PlasMag nanocomposite.

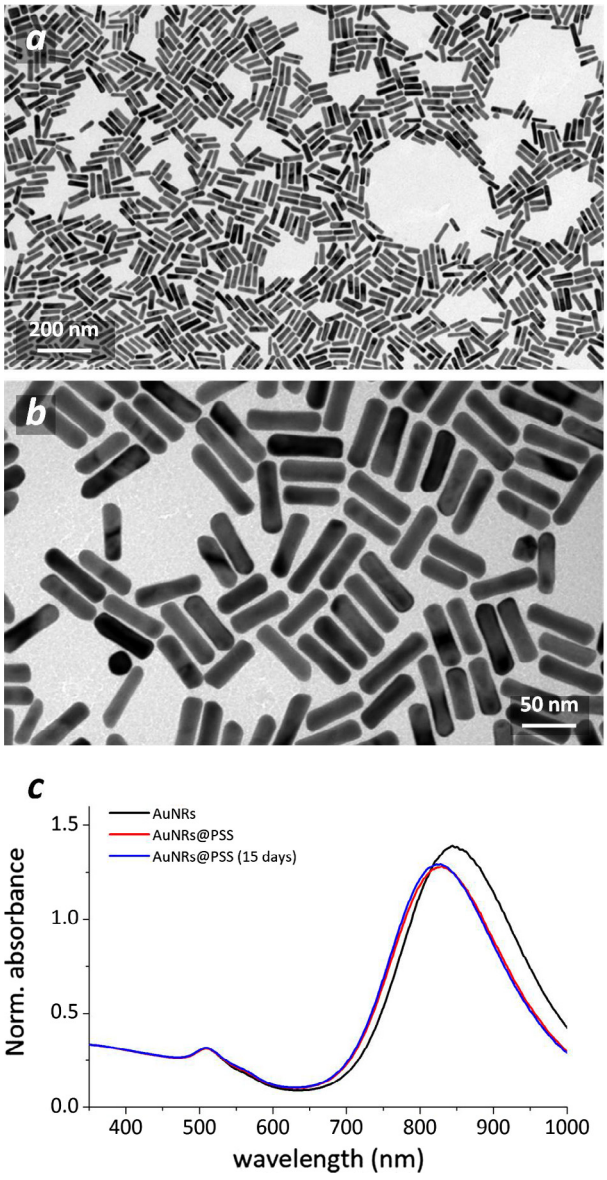

Fig. 1. (a and b) TEM images of AuNRs at different magnifications. (c) UV–Vis-NIR spectra of as prepared AuNRs (black line), PSS functionalized AuNRs (AuNRs@PSS, red line) and AuNRs@PSS after 15 days at room temperature (blue line). All the spectra have been normalized to the same value of absorbance at 400 nm to better highlight their differences. (For interpretation of the references to color in this figure legend, the reader is referred to the web version of this article.)

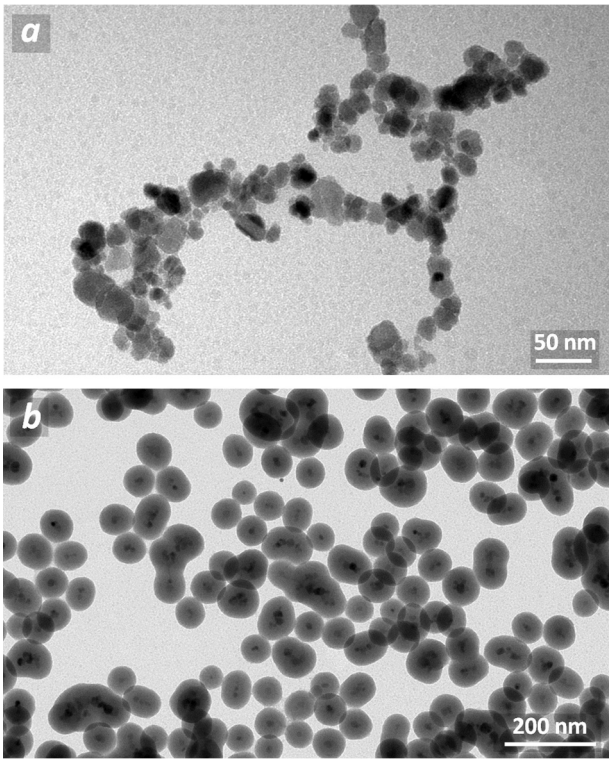

Fig. 2. TEM images of MagNPs (a) and silica-coated MagNPs, Mag@SiO_2 NPs (b).

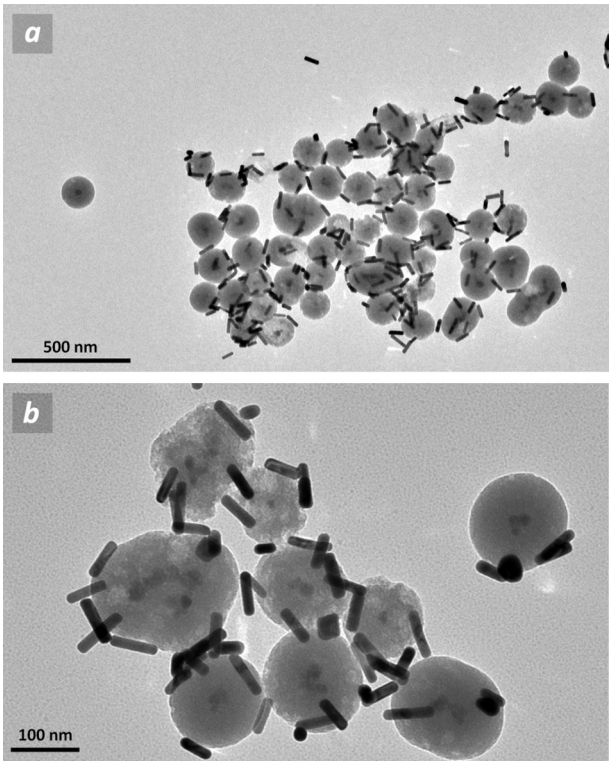

Fig. 3. TEM images of PlasMag nanocomposites at different magnifications show successful AuNRs deposition onto Mag@SiO_2 NPs.

could be explained in terms of a change in the refractive index nearby the AuNRs surface as well as the plasmon coupling occurring among Au NRs.

Furthermore, the colloidal stability in biological medium was analyzed. As showed, in Supporting Information (Fig. S2), PlasMag nanocomposites displayed poor stability in a medium such as PBS, since they aggregated and precipitated in solution even after few minutes at room temperature. To enhance the colloidal stability in PBS, the nanocomposites were coated with BSA protein. The attachment of the protein onto nanocomposite surface was confirmed by measuring the zeta-potential which changed from 14.86 ± 1.45 mV for to -9.76 ± 3.31 mV after BSA coating. BSA adsorption onto PlasMag nanocomposites probably occurs through primarily electrostatic interaction with positively charged polyelectrolyte (PEI) deposited on silica surface [30]. BSA coating provided stability to nanocomposites in biological medium even after days of storage at room temperature (see Fig. S2). The improvement of the stability is reflected in the optical response of the nanocomposites, thus the UV–vis-NIR spectra is similar to the PlasMag in water (see Fig. 4).

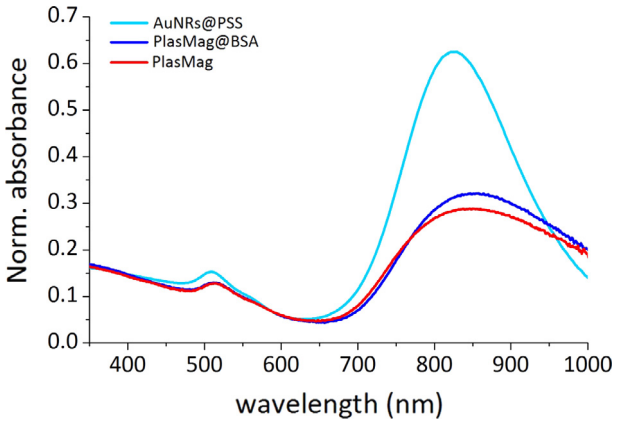

Fig. 4. Vis-NIR spectra of AuNRs@PSS (light blue line) in water, PlasMag (red line) and PlasMag@BSA (blue line) in PBS. All spectra are normalized at the same value of maximum absorbance. (For interpretation of the references to color in this figure legend, the reader is referred to the web version of this article.)

Finally, the magnetic response of the PlasMag nanocomposites was investigated. At first, we tested the magnetic character of the nanocomposite to an external magnetic field using a handmade plastic holder for either the permanent magnet and a plastic slide with a microchannel containing 500 μL of PlasMag@BSA nanocomposites in PBS. As shown in Fig. 5 the nanocomposites respond to a permanent magnetic field (1.34 T) located at the bottom of the plastic slide, demonstrating the possibility to enhance particles accumulation nearby the region of application of a permanent magnet. Nanocomposite stability is not perturbed even after magnetic accumulation, since just pipetting the PBS solution contained in the plastic channel was enough to completely redisperse them.

Moreover, magnetization *vs.* magnetic field (*M-H*) curves were recorded at 310 K for MagNPs, Mag@SiO_2 NPs and PlasMag nanocomposites to assess their magnetic response at the body temperature, relevant for *in vivo* assays. As shown in Fig. 6a and b, all three particle systems show a similar magnetization curves with saturation magnetization (M_s) of 94 emu/gFe. This indicates that silica coating and AuNRs deposition have not influenced the magnetic properties of the initial MagNPs (amino-functionalized iron oxide NPs). Besides, all particles show coercive fields (H_c) of 4.5–5 mT at 310 K. As expected, the particles exhibit a higher magnetization at 10 K as a result of a better alignment along the field at lower temperatures (Fig. 6c). Note that the blocking temperature (T_b) of the particles, estimated from ZFC-FC curves (Fig. 6d), was not affected by silica coating and AuNRs assembly processes as it remains around 225 K for all the samples. This, also implies that the pristine magnetic properties are preserved once encapsulated in the final plasmonic-magnetic nanostructures. Finally, the final nanostructures are superparamagnetic at room temperature with a remarkably high magnetic response and a great potential for magnetic manipulation.

3.4. Photothermal behavior of PlasMag@BSA nanocomposites

Photothermal behavior by PlasMag@BSA nanocomposites has been investigated in order to evaluate their possible use for ablative cancer therapy. Thus, liquid samples containing a defined concentration of PlasMAg@BSA nanocomposites have been irradiated witha NIR laser source (70 mW, λ = 808 nm, which overlaps with the LSPR of the nanocomposites) and thermal images were recorded with an IR thermocamera. As shown in Fig. 7, NIR laser stimulation determines an increase in sample temperature that spreads over the spot of the focused NIR laser. In particular, when laser is focused on the top of a 2 μL drop of PlasMag@BSA nanoparticles in PBS, an instantaneous temperature rise is detected and temperature spreading towards the drop volume and the underlying plastic slide is observed (Fig. 7a). Temperature recorded at the centre of the drop rises from 24.5 °C up to 40 °C after around 40 s of laser stimulation, and decreases exponentially after laser switching OFF. Heating effect is due to the dissipation of the absorbed light energy guaranteed by strong NIR photons absorption of complexed AuNRs onto silica-coated magnetic nanoparticles. Interestingly, the temperature distribution reaches a steady state after around 30 s of laser action onto the nanoparticles drops. This effect is a result of the thermal exchange among PlasMag@BSA nanoparticles, the aqueous medium and the surrounding environment, that reaches equilibrium after few seconds of laser action. Conversely, laser stimulation of a drop of Mag@SiO_2 or PBS resulted in a very small temperature increase, around 2 °C, (see Supporting Information, Fig. S3), due to very low absorption cross section of Mag@SiO_2

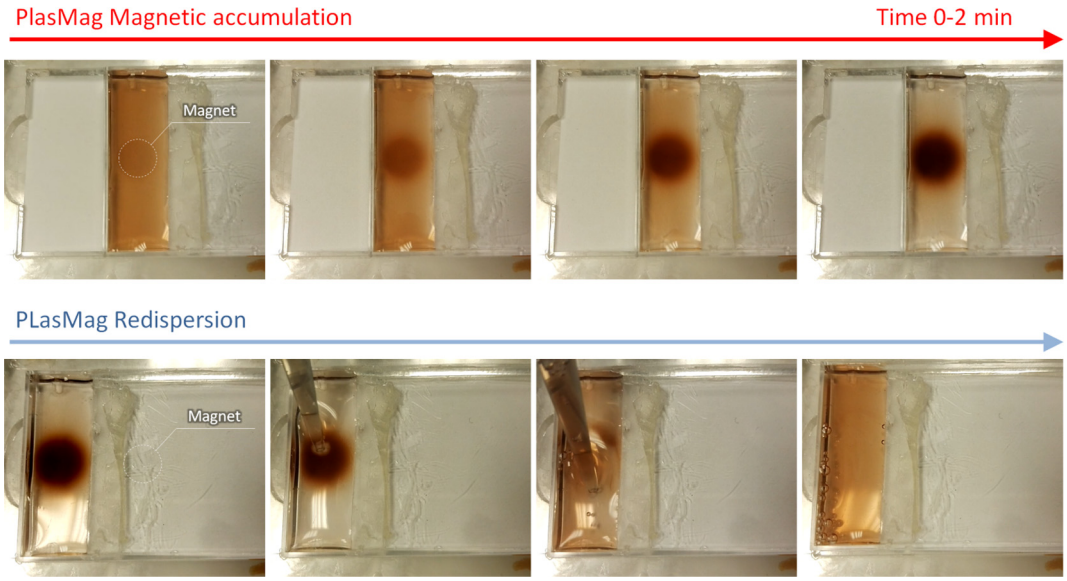

Fig. 5. Magnetic behavior of PlasMag@BSA nanocomposites recorded in time-lapse. Almost complete nanoparticles accumulation was possible after 2 min of permanent magnet application at the bottom of the plastic slide. Successful particles resuspension was possible after magnetic accumulation (see also Supplementary Video).

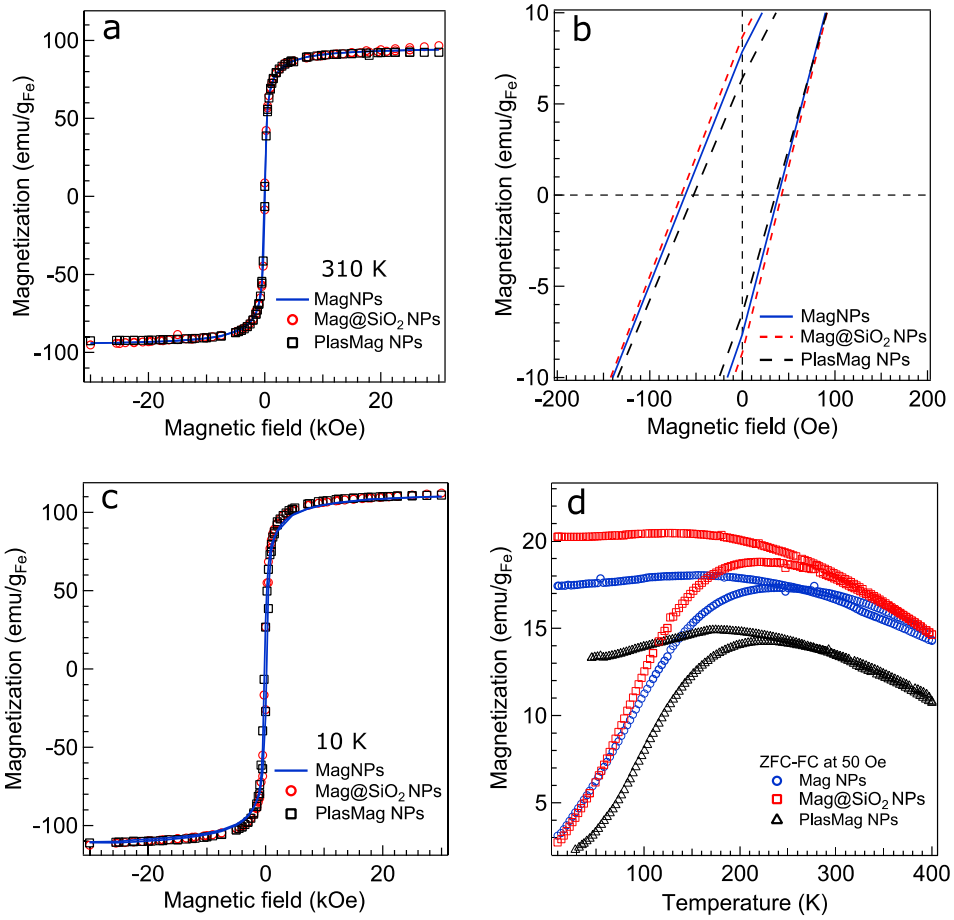

Fig. 6. (a–c) Magnetization versus magnetic field recorded at 310 K (full range in a; zoomed view in b) and 10 K (c) for MagNPs, Mag@SiO_2 NPs and PlasMag nanocomposites. (d) zero-field-cooled (ZFC) and field-cooled (FC) magnetization curves recorded at 50 Oe cooling fields for MagNPs, Mag@SiO_2 NPs and PlasMag nanocomposites. All values are normalized to the particle iron concentration.

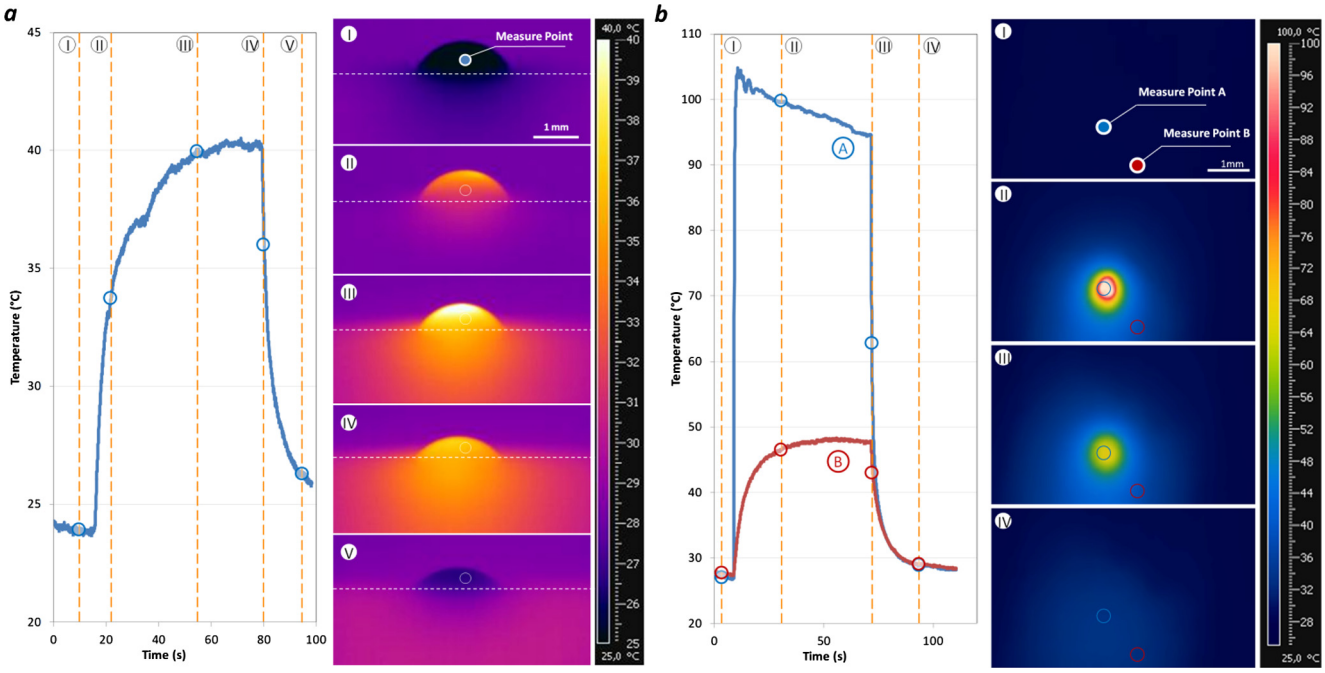

Fig. 7. Photothermal behavior of PlasMag@BSA nanocomposites. (a) Thermal images (lateral view) of a 2 μL drop of 2 mg/mL PlasMag@BSA nanocomposites in PBS placed onto a Plexiglas support at different time frames (λ = 808 nm, 70 mW) and relative plot of temperature vs irradiation time. (b) Thermal images (top view) and plot of temperature vs irradiation time of PlasMag@BSA nanocomposites under NIR laser stimulation (λ = 808 nm, 70 mW) after magnetic accumulation and excess PBS solution removal.

NPs and PBS. This demonstrates that the thermal effect is substantially given by Au nanorods contained in the PlasMag@BSA nanocomposites.

Finally, in order to verify the influence of magnetic accumulation on thermal properties of a nanoparticle dispersion we also investigated the effect of laser stimulation on a concentrated sample of PlasMag@BSA nanoparticles, obtained by magnetic accumulation (Fig. 7b). Magnetic accumulation is performed with the setup shown in Fig. 5. Besides we measured the temperature during irradiation time at the laser spot (Point A, in Fig. 7b) and at 1 mm far away from the centre of temperature distribution (Point B, in Fig. 7b). The results reveal a sharp increase of maximum temperature at Point A almost instantaneously, since temperature reaches 104 °C in less than one second. Then a constant decrease of maximum temperature at the laser spot is observed and explained in terms of residual PBS evaporation. Temperature recording at Point B showed a less drastic rise and evidenced the achievement of a steady state of temperature rise after around 30 s of laser action. Exponential temperature decrease has been observed at Point A and B after laser switching OFF. Furthermore, thermal images revealed a localized temperature spreading during laser action, with temperature that exponentially diminishes below 40 °C at 1.05 mm far away from the edge of maximum recorded temperature. Finally, laser excitation of magnetically accumulated Mag@SiO_2 NPs (without Au nanorods) determined an almost negligible temperature rise of 1 °C confirming the very poor NIR photon absorption of these nanoparticles.

These results demonstrated that attachment of gold nanorods onto silica-coated magnetic nanoparticles plays a central role in NIR photon absorption and consequent environmental temperature rise during laser stimulation of PlasMag@BSA NPs. A small amount of AuNRs onto silica surface resulted to be enough to increase local temperature using an output laser power of 70 mW. Although a remarkable photothermal response is observed either with or without magnetic accumulation of hybrids, the effect is stronger through the magnetic accumulation of PlasMag@BSA NPs. This occurrence showed that, in the optic of a clinical use of these nanoparticles, magnetic accumulation could not only affect nanoparticles cellular uptake, but also drastically influence photothermal behavior, allowing to obtain a much more intense and controlled localized heating compared to generic nanoparticles active targeting.

4. Conclusions

In this work the possibility to fabricate a nanocomposite assembly that could couple plasmonic and magnetic characteristic has been demonstrated. Silica coating onto magnetic nanoparticles has been provided in order to improve surface chemistry of magnetic nanoparticles thus preventing aggregation. Polyelectrolyte coating of either silica-coated magnetic nanoparticles and gold nanorods has been used to exploit electrostatic interactions that allowed PlasMag formations. BSA coating of the nanocomposite provided good colloidal stability in biological medium that prevented nanoparticles irreversible aggregation, which were stable at room temperature for several days. Optical characterization showed the presence of a plasmonic band in the near infrared region of light spectrum with the maximum absorbance value around at 840 nm. Moreover, the possibility to increase nanocomposite concentration was demonstrated by using an external magnetic field of around 1.32 T. Magnetic characterization of PlasMag@BSA showed a superparamagnetic behavior at room temperature and a saturation magnetization value that lead good potential for magnetic manipulation for our nanocomposite. Furthermore, photothermal behavior of our nanocomposite revealed localized and strong absorbed energy conversion and subsequent environmental heating with respect to control experiments, demonstrating that AuNRs complexation onto silica-coated nanoparticles plays the central role in photothermal energy conversion. Temperature recording upon magnetic accumulation of PlasMag@BSA showed intense heating with maximum temperatures that exceeded 100 °C in a few milliseconds with an output laser power of 70 mW. This occurrence demonstrated that nanocomposite local increased concentration due to magnetic accumulation could be an advantageous strategy to influence photothermal energy conversion and nanoparticles targeting during systemic administration of PlasMag@BSA.

These evidences displayed the formation of a stable nanocomposite that could be used for photothermal ablation of tumor masses upon intravenous injection and magnetic accumulation. Further *in vivo* experiments will be required in order to test the possibility to destroy a tumor mass upon NIR laser stimulation after magnetic accumulation of the nanomaterial.

Acknowledgments

The authors would like to thank Dr. Ricardo Andrade, Dr. Stefanos Mourdikoudis and Dr. Guangchao Zheng for their assistance for TEM imaging. This work was supported by the Spanish MINECO (MAT2016-77809-R).

Appendix A. Supplementary material

Supplementary data associated with this article can be found, in the online version, at http://dx.doi.org/10.1016/j.jcis.2017.04.089.

References

[1] E. Hutter, J.H. Fendler, Exploitation of localized surface plasmon resonance, Adv. Mater. 16 (2004) 1685–1706, http://dx.doi.org/10.1002/adma.200400271.
[2] C. Burda, X. Chen, R. Narayanan, M.A. El-Sayed, Chemistry and properties of nanocrystals of different shapes, 2005. http://dx.doi.org/10.1021/cr030063a.
[3] J. Perezjuste, I. Pastorizasantos, L. Lizmarzan, P. Mulvaney, Gold nanorods: synthesis, characterization and applications, Coord. Chem. Rev. 249 (2005) 1870–1901, http://dx.doi.org/10.1016/j.ccr.2005.01.030.
[4] a. Sánchez-Iglesias, I. Pastoriza-Santos, J. Pérez-Juste, B. Rodríguez-González, F. J. García de Abajo, L.M. Liz-Marzán, Synthesis and optical properties of gold nanodecahedra with size control, Adv. Mater. 18 (2006) 2529–2534, http://dx.doi.org/10.1002/adma.200600475.
[5] P. Senthil Kumar, I. Pastoriza-Santos, B. Rodríguez-González, F. Javier García de Abajo, L.M. Liz-Marzán, High-yield synthesis and optical response of gold nanostars, Nanotechnology 19 (2008) 15606, http://dx.doi.org/10.1088/0957-4484/19/01/015606.
[6] S. Barbosa, A. Agrawal, L. Rodríguez-Lorenzo, I. Pastoriza-Santos, R.A. Alvarez-Puebla, A. Kornowski, et al., Tuning size and sensing properties in colloidal gold nanostars, Langmuir 26 (2010) 14943–14950, http://dx.doi.org/10.1021/la102559e.
[7] N. Pazos-Pérez, S. Barbosa, L. Rodríguez-Lorenzo, P. Aldeanueva-Potel, J. Pérez-Juste, I. Pastoriza-Santos, et al., Growth of sharp tips on gold nanowires leads to increased surface-enhanced Raman scattering activity, J. Phys. Chem. Lett. 1 (2010) 24–27, http://dx.doi.org/10.1021/jz900004h.
[8] A. Guerrero-Martínez, J. Pérez-Juste, L.M. Liz-Marzán, Recent progress on silica coating of nanoparticles and related nanomaterials, Adv. Mater. 22 (2010) 1182–1195, http://dx.doi.org/10.1002/adma.200901263.
[9] J.-M. Nam, Amit Kumar, Sungi Kim, Plasmonically engineered nanoprobes for biomedical applications, J. Am. Chem. Soc. 44 (2016) 14509–14525.
[10] C.J. Murphy, M.A. El-Sayed, Erik C. Dreaden, Alaaldin M. Alkilany, Xiaohua Huang, The golden age: gold nanoparticles for biomedicine, Chem. Soc. Rev. 41 (2012) 2740–2779.
[11] Y.C. Cao, R. Jin, C.A. Mirkin, Nanoparticles with Raman spectroscopic fingerprints for DNA and RNA detection, Science 297 (2002) 1536–1540.
[12] I. Pavel, E. Mccarney, A. Elkhaled, A. Morrill, K. Plaxco, M. Moskovits, NIH public access, J. Phys. (Main Title) 112 (2009) 4880–4883, http://dx.doi.org/10.1021/jp710261y.Label-Free.
[13] L. Rodríguez-Lorenzo, Z. Krpetic, S. Barbosa, R.a. Alvarez-Puebla, L.M. Liz-Marzán, I.a. Prior, et al., Intracellular mapping with SERS-encoded gold nanostars, Integr. Biol. (Camb.) 3 (2011) 922–926, http://dx.doi.org/10.1039/c1ib00029b.
[14] D.P. O'Neal, L.R. Hirsch, N.J. Halas, J.D. Payne, J.L. West, Photo-thermal tumor ablation in mice using near infrared-absorbing nanoparticles, Cancer Lett. 209 (2004) 171–176, http://dx.doi.org/10.1016/j.canlet.2004.02.004.

[15] C. Loo, A. Lin, L. Hirsch, M.-H. Lee, J. Barton, N. Halas, et al., Nanoshell-enabled photonics-based imaging and therapy of cancer, Technol. Cancer Res. Treat. 3 (2004) 33–40. <http://www.ncbi.nlm.nih.gov/pubmed/14750891>.
[16] L.R. Hirsch, R.J. Stafford, J.A. Bankson, S.R. Sershen, B. Rivera, R.E. Price, et al., Nanoshell-mediated near-infrared thermal therapy of tumors under magnetic resonance guidance, Proc. Natl. Acad. Sci. USA 100 (2003) 13549–13554, http://dx.doi.org/10.1073/pnas.2232479100.
[17] D.P. O'Neal, L.R. Hirsch, N.J. Halas, J.D. Payne, J.L. West, Photo-thermal tumor ablation in mice using near infrared-absorbing nanoparticles, Cancer Lett. 209 (2004) 171–176, http://dx.doi.org/10.1016/j.canlet.2004.02.004.
[18] X.H. Huang, I.H. El-Sayed, W. Qian, M.a. El-Sayed, Cancer cell imaging and photothermal therapy in the near-infrared region by using gold nanorods, J. Am. Chem. Soc. 128 (2006) 2115–2120, http://dx.doi.org/10.1021/ja057254a.
[19] E.S. Day, P.A. Thompson, L. Zhang, N.A. Lewinski, N. Ahmed, R.A. Drezek, et al., Nanoshell-mediated photothermal therapy improves survival in a murine glioma model, J. Neurooncol. 104 (2011) 55–63, http://dx.doi.org/10.1007/s11060-010-0470-8.
[20] E.R. Riva, A. Desii, E. Sinibaldi, G. Ciofani, V. Piazza, B. Mazzolai, et al., Gold nanoshell/polysaccharide nano fi lm for controlled laser-assisted tissue thermal ablation, ACS Nano (2014) 5552–5563.
[21] N. Khlebtsov, L. Dykman, Biodistribution and toxicity of engineered gold nanoparticles: a review of in vitro and in vivo studies, Chem. Soc. Rev. 40 (2011) 1647–1671, http://dx.doi.org/10.1039/c0cs00018c.
[22] A.J. Cole, V.C. Yang, A.E. David, Cancer theranostics: the rise of targeted magnetic nanoparticles, Trends Biotechnol. 29 (2011) 323–332, http://dx.doi.org/10.1016/j.tibtech.2011.03.001.
[23] J. Kim, S. Park, J.E. Lee, S.M. Jin, J.H. Lee, I.S. Lee, et al., Designed fabrication of multifunctional magnetic gold nanoshells and their application to magnetic resonance imaging and photothermal therapy, Angew. Chem. – Int. Ed. 45 (2006) 7754–7758, http://dx.doi.org/10.1002/anie.200602471.
[24] J. Lee, J. Yang, H. Ko, S. Oh, J. Kang, J. Son, et al., Multifunctional magnetic gold nanocomposites: human epithelial cancer detection via magnetic resonance imaging and localized synchronous therapy, Adv. Funct. Mater. 18 (2008) 258–264, http://dx.doi.org/10.1002/adfm.200700482.
[25] P.K. Jain, K.S. Lee, I.H. El-Sayed, M.A. El-Sayed, Calculated absorption and scattering properties of gold nanoparticles of different size, shape, and composition: applications in biological imaging and biomedicine, J. Phys. Chem. B 110 (2006) 7238–7248, http://dx.doi.org/10.1021/jp057170o.
[26] N. Zhou, L. Polavarapu, N. Gao, Y. Pan, Electronic supplementary information TiO_2 coated Au/Ag nanorods with enhanced photocatalytic activity under visible light irradiation, Nanoscale 5 (10) (2013) 4236–4241.
[27] I. Pastoriza-Santos, J. Pérez-Juste, L.M. Liz-Marzán, Silica-coating and hydrophobation of CTAB-stabilized gold nanorods, Chem. Mater. 18 (2006) 2465–2467, http://dx.doi.org/10.1021/cm060293g.
[28] W. Stöber, A. Fink, E. Bohn, Controlled growth of monodisperse silica spheres in the micron size range, J. Colloid Interf. Sci. 26 (1968) 62–69, http://dx.doi.org/10.1016/0021-9797(68)90272-5.
[29] M.A. Correa-duarte, M. Farle, A. Lo, K. Sieradzki, R. Diaz, A. State, et al., Bifunctional gold-coated magnetic silica spheres, Chem. Mater. (2006) 2701–2706.
[30] V. Ball, B. Szalontai, Y. Haikel, J. Voegel, P. Schaaf, Secondary structure of proteins adsorbed onto or embedded in polyelectrolyte multilayers, Biomacromolecules (2002) 1135–1143.